Available online at www.sciencedirect.com
SCIENCE DIRECT®
Polymer 45 (2004) 3341–3349
polymer
www.elsevier.com/locate/polymer

Nanoindentation and morphological studies on nylon 66 nanocomposites. I. Effect of clay loading

Lu Shen, In Yee Phang, Ling Chen, Tianxi Liu*, Kaiyang Zeng

Institute of Materials Research and Engineering, 3 Research Link, Singapore 117602, Singapore

Received 9 November 2003; received in revised form 11 March 2004; accepted 12 March 2004

Abstract

Nanoindentation technique has been used to investigate the mechanical properties of exfoliated nylon 66 (PA66)/clay nanocomposites in present study. The hardness, elastic modulus and creep behavior of the nanocomposites have been evaluated as a function of clay concentration. It indicates that incorporation of clay nanofiller enhances the hardness and elastic modulus of the matrix. The elastic modulus data calculated from indentation load-displacement experiments are comparable with those obtained from dynamic mechanical analysis and the tensile tests. However, the creep behavior of the nanocomposites shows an unexpected increasing trend as the clay loading increases (up to 5 wt%). The lowered creep resistance with increasing clay content is mainly due to the decrease of crystal size and degree of crystallinity as a result of clay addition into PA66 matrix, as evidenced by optical microscopy and X-ray diffraction. At lower clay concentration (here $\leq$5 wt%), morphological changes due to addition of clay plays the dominant role in creep behavior compared with the reinforcement effect from nanoclay.

Keywords: Nylon 66; Nanocomposites; Nanoindentation

1. Introduction

During the past decade, polymer nanocomposites have attracted much interest in both commercial research organizations and academic laboratories. In the late 1980s, the researchers from Toyota successfully developed polyamide 6/organophilic montmorillonite clay nanocomposites by in-situ polymerization [1–2]. Compared with their neat counterparts, the nanocomposites show greatly improved physical properties including tensile strength, modulus, heat distortion temperature, fire retardancy and gas permeability [1–4], due to the large surface area of the clay platelets and their fine dispersion within the polymeric matrices. The preparation methods of polymer/clay nanocomposites are mainly divided into three groups according to the starting materials and processing techniques: intercalation of polymer or pre-polymer from solution, in situ intercalative polymerization method, and melt intercalation method [5]. The melt intercalation approach involves annealing (statically) or melt-compounding (under shear flow), a mixture of the polymer and organically modified clay (organoclay) above softening or melting point of the polymer [6]. Under these conditions and if the layer surfaces are sufficiently compatible with the chosen polymer, the (molten) polymer chains can crawl into the interlayer galleries and form either an intercalated or an exfoliated nanocomposites according to the degree of penetration. This method has more advantages than either in situ intercalative polymerization or polymer solution intercalation. First, this method is environmentally benign due to the absence of organic solvents. Second, it is compatible with conventional industrial processes, such as extrusion and injection molding and other polymer processing techniques, thus being easily commercialized. And, the melt intercalation method allows the use of polymers which were previously not suitable for in situ polymerization or solution intercalation [5].

Nanoindentation is a new and advanced technique, which can provide a wealth of valuable quantitative information regarding the mechanical properties of a variety of materials (e.g. thin films) at the very first surface layers [7,8]. This method relies on the local deformation induced on a material surface using an indenter with known geometry

* Corresponding author. Tel.: +65-68748594; fax: +65-67744657.
E-mail address: liu-tx@imre.a-star.edu.sg (T. Liu).

0032-3861/$ - see front matter © 2004 Elsevier Ltd. All rights reserved.
doi:10.1016/j.polymer.2004.03.036

under the application of a given load. In an indentation experiment, the yield stress is exceeded and the indentation depth variation is a combination of both the viscoelastic and viscoplastic contributions to the total indentation depth. In the past decade, nanoindentation method has been employed extensively to characterize the mechanical properties of various materials, especially inorganic substances [8]. And only most recently, this powerful but simple analytical technique began to be employed into polymeric systems [9,10], such as in polyvinylchloride, poly(ethylene oxide), poly(acrylic acid) [11], poly(ethylene terephthalate) [8,12,13], nylon 6 and their blends or composites [14]. In spite of these, nanoindentation is surprisingly seldom utilized to probe the micro- and/or nano-mechanical behavior of polymer nanocomposites [15], for instance, in polymer/clay nanocomposite systems [16]. And the understanding in these aspects is so far wretchedly lacking and limited. Therefore, it is expected that the application of nanoindentation into polymer nanocomposites could provide more useful information, and thus make people get deeper fundamental understanding in the improved properties as well as the enhancement mechanism(s) resulting from the nanoscale fillers.

Recently, more studies on the preparation and structure (particularly crystal transition or polymorphism) of nylon 66/clay nanocomposites have been reported [17–24], as the overall properties of nylon 66 are superior to those of nylon 6. However, less attention is paid to the mechanical properties of nylon 66/clay nanocomposites [19,24], never mentioned to the elastic properties investigated by means of nanoindentation. In present study, the elastic modulus, hardness and creep behavior of PA66 and its nanocomposites prepared by melt compounding have been studied by nanoindentation experiments as a function of clay loading. An attempt has been made to correlate the observed mechanical properties with the enhancing effect from nanoclay as well as the morphological changes due to addition of nanoclay into the matrix.

2. Experimental

2.1. Materials and sample preparation

Neat nylon 66 (PA66) pellets (EPR32, with relative viscosity of 3.2) used in this study were kindly provided by China Shenma Group Co. Ltd. Organoclay, Nanomer® I.34TCN (from Nanocor Inc., USA), is a surface modified montmorillonite mineral with a mean particle size of 16–22 μm, which is specifically designed for extrusion compounding and usually used in nylon 6 and nylon 66 systems [25]. PA66 nanocomposites with different clay concentrations (up to 5 wt%) were prepared by melt-compounding using Brabender twin-screw extruder at 280 °C with a screw speed of 180 rpm, followed by pelletizing. The pelletized materials were dried and injection molded into rectangular bars with dimension of $12.5 \times 6.5 \times 160$ mm^3. The detailed studies on preparation, structure/morphology, thermal and mechanical properties of PA66/clay nanocomposites have been reported elsewhere [26]. The specimens were then cut into small pieces suitable for nanoindentation tests. After that, the sample surfaces parallel to the injection flow direction were polished using SiC paper in order to remove or eliminate the processing induced defects or other artifacts (for example, till no discernible scratches are observed under optical microscope). After being dried in oven at 80 °C for about 24 h, the polished samples were mounted on aluminum stub using super glue for subsequent indentation tests.

2.2. Morphology by microscopy, X-ray diffraction and thermal analysis

Ultrathin films (with thickness of about 80 nm) for transmission electron microscopy (TEM) observation was prepared by cutting from the trimmed surface perpendicular to flow direction using a diamond knife with Leica Ultracut UCT microtome at −80 °C. The sections were then collected on carbon coated copper grids. A Philips CM300-FEG TEM operating at an accelerating voltage of 150 kV was used to examine the morphology.

The films used for optical microscopy observations were prepared by melting (at 280 °C for 5 min) and pressing small amounts of extruded neat PA66 and the nanocomposite with 1 wt% clay (sandwiched between two microscope glass slides) and then cooling to 80 °C for annealing for 24 h. The crystalline morphologies of the obtained film samples (with thickness of about 50 μm) were observed using polarized light microscope (POM) (Olympus BX60 system).

X-ray diffraction (XRD) patterns of the samples having same thermal history as those for POM observations were recorded using a Bruker GADDS diffractometer equipped with an area detector, operating at a voltage of 40 kV and current of 40 mA using a Cu K_α radiation ($\lambda = 0.15418$ nm).

Differential scanning calorimetric (DSC) was performed under nitrogen flow from room temperature to 300 °C at a scanning rate of 10 °C/min by using a TA MDSC 2900. Three sets of the samples were taken from different locations (i.e. surface, intermediate and core parts) of the injection-molded bulk specimens. The weights of samples varied from 4 to 6 mg. The degree of crystallinity was estimated by dividing the enthalpies of the samples by the heat of fusion ($\Delta H_m^0 = 206$ J/g [27]) of fully crystalline PA66.

2.3. Tensile testing

The tensile tests were carried out using an Instron tensile machine (Model 5567) at room temperature. The gauge length was set as 50 mm and the crosshead speed was 5 mm/min. An extensometer (Model 2630-105) was used to

accurately determine the elastic modulus from the initial part of stress–strain curves. At least six specimens of each composition were tested.

2.4. Nanoindentation experiments

The nanoindentation tests were performed on MTS Nano Indenter® XP (MTS Cooperation, Nano Instruments Innovation Center, TN, USA) with a continuous stiffness measurement technique [28]. In this technique, an oscillated force with known frequency and amplitude was superimposed onto the nominal applied force. The material, which is in contact with the oscillated force, responds with a displacement phase and amplitude. The materials stiffness (S) and damping (ωC) along indentation loading can be calculated using Eqs. (1) and (2), respectively. The hardness and elastic modulus are calculated using stiffness data from Eqs. (3) and (4), respectively. Therefore, the hardness and modulus are determined as a function of indentation depth with a single loading/unloading cycle.

$$S = \left[\frac{1}{\frac{P_{\max}}{h(\omega)} \cos \Phi - (K_s - m\omega^2)} - K_f^{-1} \right]^{-1} \quad (1)$$

$$\omega C = \frac{P_0}{h(\omega)} \sin \Phi \quad (2)$$

$$\frac{E}{1-\nu^2} = \frac{\sqrt{\pi}}{2} \frac{1}{\sqrt{A_c}} S \quad (3)$$

$$H = \frac{P_{\max}}{A_c} \quad (4)$$

where $P_{\max}$ and $h(\omega)$ are driving force and the displacement response of the indenter, respectively; Φ is the phase angle between $P_{\max}$ and $h(\omega)$; m is mass of the indenter column; K_s is spring constant at the vertical direction; K_f is frame stiffness. m, K_s and K_f are all constant values for specified indentation system. ω is angle speed which equals to $2\pi f$; f is the driven frequency of the AC signal. ν is Possion's ratio and set to be 0.35 for current analysis [14]. A_c is contact area at the moment material in contact with indenter with load $P_{\max}$.

A three-side pyramid (Berkovich) diamond indenter was employed for the indentation experiments. The area function, which is used to calculate contact area A_c from contact depth h_c, was carefully calibrated using standard sample, fused silica, before the experiments. The nanoindentation tests were carried out in following sequence: firstly, after the indenter in contact with the surface, it was approaching into the material with constant strain rate, i.e. 0.05 1/s, until 5000 nm deep into surface; secondly, the load was held at maximum value for 60 s in order to study the creep behavior; and finally, the indenter was withdrawn from the surface with same rate as loading until 10% of the maximum load. Before indenter totally withdrawn from the sample surface, another hold for 60 s was performed to monitor the creep recovery behavior [29]. Here, constant strain rate was chosen to load on the samples in order to avoid strain hardening effect on the measurements [16]. At least 10 indents were performed on each sample and the interval of each two indents was 50 μm to avoid interaction. Additionally, in order to evaluate the polishing effect on the mechanical properties of PA66 and its nanocomposite systems by nanoindentation, a set of unpolished samples was also tested for comparison.

3. Results and discussion

As an example, Fig. 1 shows TEM micrographs for PA66 nanocomposite containing 5 wt% clay. An overall TEM image at low magnification as shown in Fig. 1(A) shows a very fine dispersion of the nanoclay platelets (dark lines, with an aspect ratio of about 200) throughout the matrix. TEM image at higher magnification more clearly shows that delaminated or exfoliated clay morphology within PA66 matrix has been successfully achieved by melt compounding. Detailed studies on the nanostructure, thermal and mechanical properties of PA66/clay nanocomposites prepared are reported elsewhere [26].

Fig. 2(A) shows the representative stress-strain curves of PA66/clay nanocomposites. All the nanocomposites exhibit post yield elongation. The Young's modulus and tensile strength are plotted in Fig. 2(B) as a function of clay content. Both the Young's modulus and tensile strength steadily increased with clay content. It is noteworthy that tensile modulus increases by 30% and tensile strength by 16% with the addition of 5 wt% clay to PA66, which is consistent with Kojima's findings [2] on nylon 6/clay nanocomposites. The role of clay as a reinforcing agent in PA66 matrix is clearly manifested. The property improvements reported here are higher than that reported by Chen et al. for maleic anhydride modified polypropylene (MAPP)/organoclay nanocomposites [30], implying that interfacial bonding between layered silicates and PA66 is more stronger. However, a comprehensive understanding of the interfacial interaction between PA66 and organoclay is lacking. We believe that the higher parity between the surface polarities of PA66 and organoclay leads to platelet exfoliation of clay among the polymer matrix, resulting in more efficient reinforcement effect. The elongation at break of the nanocomposites decreases from about 180% (for neat PA66) to 25% (with 5 wt% clay), indicating that the plastic deformation of matrix is severely curtailed with the incorporation of clay leading to embrittlement. Future work will focus on the deformation behavior of PA66/clay nanocomposites and the establishment of embrittlement mechanisms using microscopy techniques.

Fig. 3 shows typical loading-hold-unloading curves of neat PA66 and its nanocomposites as a function of clay content. On loading, the forces are incremented at constant

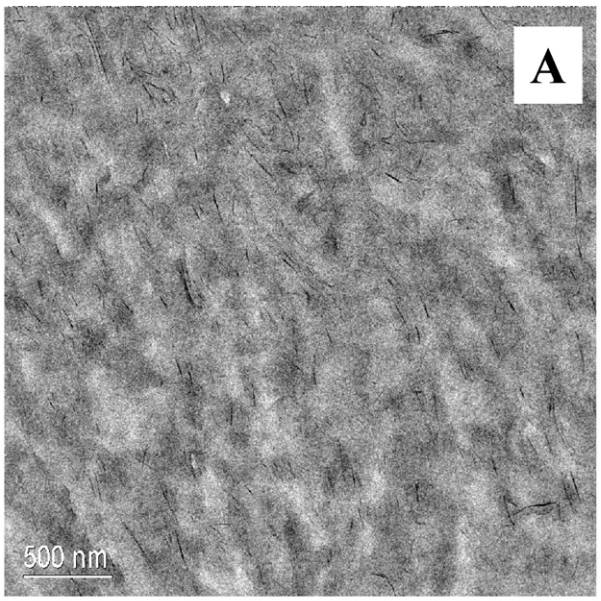

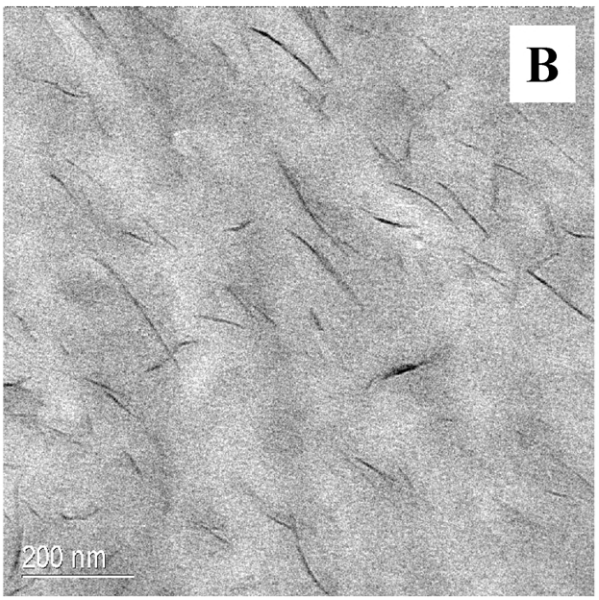

Fig. 1. TEM images showing exfoliated clay morphology for PA66 nanocomposite containing 5 wt% clay. (A) Low magnification; (B) high magnification.

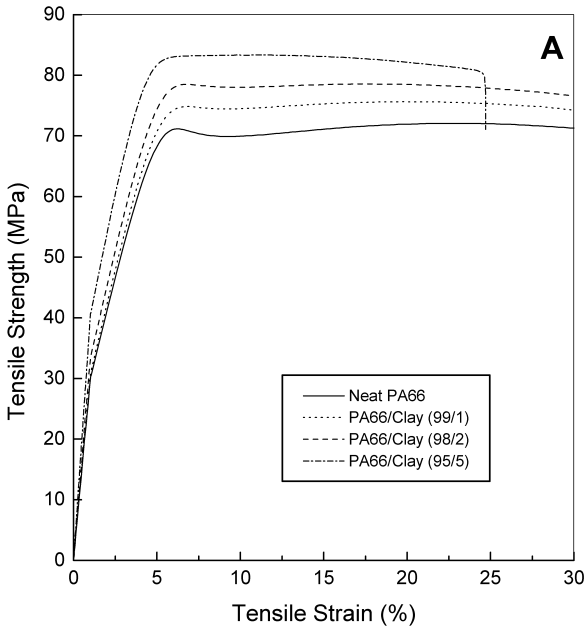

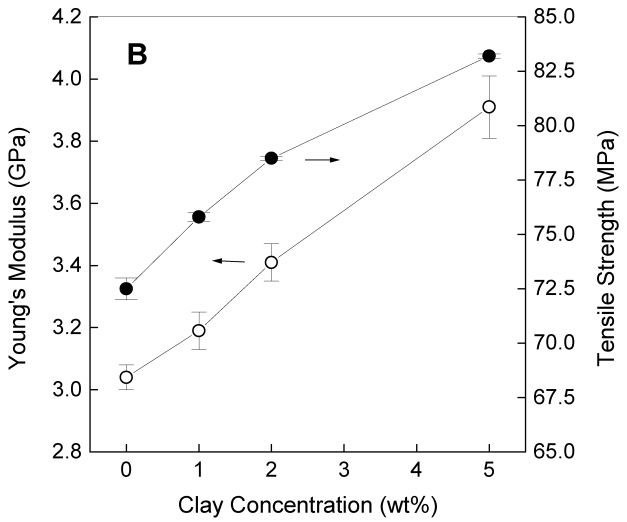

Fig. 2. (A) Stress–strain curves for nylon 66 and its clay nanocomposites at a crosshead speed of 5 mm/min; (B) tensile modulus (E) and yield strength (σ_y) of PA66/clay nanocomposites as a function of clay concentration.

velocities. The curves steadily shift upwards with increasing the clay concentration, indicating that the nanocomposites' resistance to indentation gradually increases with clay concentration. The depths represent the contributions from both the elastic and the plastic displacements. The loading curves are followed by a period of holding time (here, 60 s) at which the peak loads are kept constant. During unloading, the load is reduced at the same rate as in the loading cycle. In this case, the elastic displacements are recovered. It can be seen that significant creep was clearly found in the maximum hold segments for both neat PA66 and the nanocomposites. In particular, the (creep) depths or displacements steadily increase with increasing clay content, suggesting that increasing clay concentration (up to 5 wt%) deteriorates the creep resistance of the materials. Details of this unexpected creep behavior for the nanocomposites will be discussed later.

Figs. 4(A) and (B) shows the hardness and modulus profiles with respect to the indentation depth, respectively, for neat PA66 and the nanocomposites. It can be seen that both the hardness and the elastic modulus are enhanced as a function of clay concentration, due to the addition of stiff nanoclay fillers into the matrix. The dramatic drops of the hardness and the modulus before 200 nm are probably due to the indentation size effect [31]. There are several possible origins for the indentation size effect, such as: (1) the

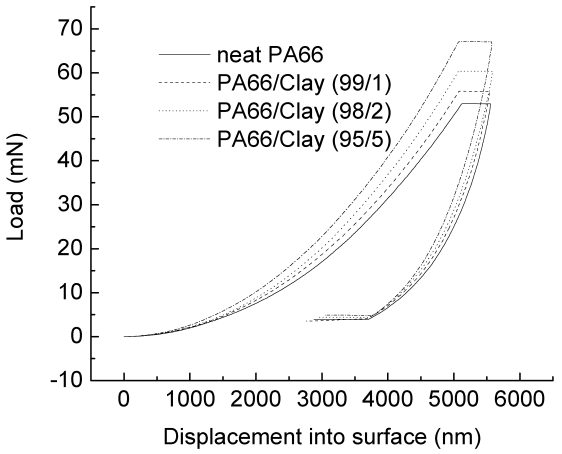

Fig. 3. Typical loading-hold-unloading curves of neat PA66 and PA66/clay nanocomposites.

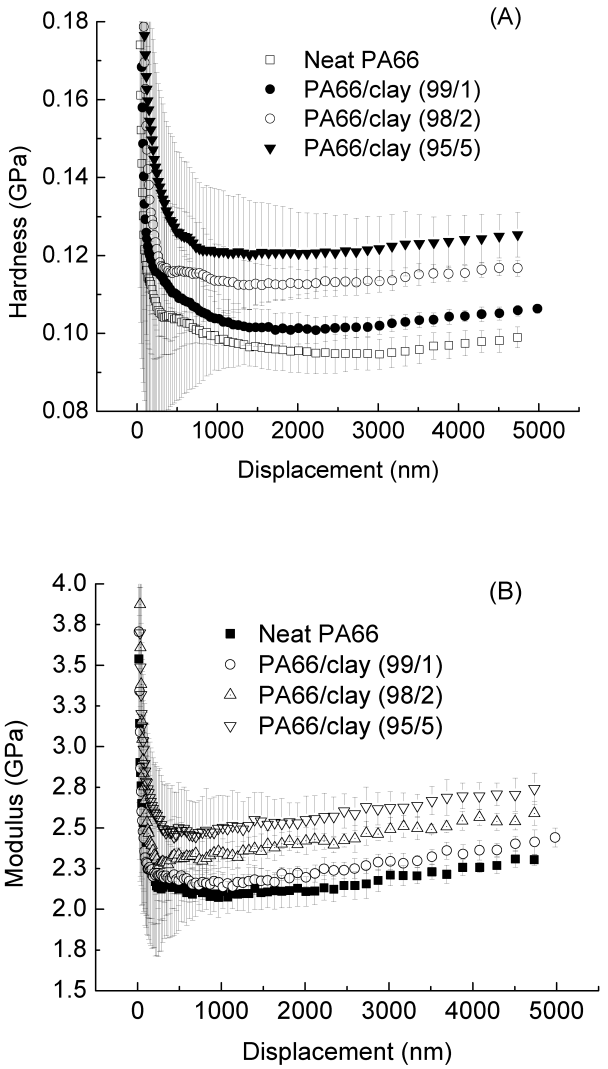

Fig. 4. Hardness and modulus profiles of PA66 as a function of clay loading. (A) Hardness profile; (B) modulus profile.

blunting of the tip at the apex of the indenter leads to unavoidable over-estimate of the hardness and modulus at the near-surface area, (2) the inaccuracy of the indenter area function determination at low depth, and (3) the inaccuracy in sample surface finding segment at the initial loading portion. For the case of the hardness (Fig. 4(A)), from 400 nm onwards, the hardness profiles of the samples roughly stabilize at certain values between 1000 and 3000 nm followed by a modest but steady increase after 3000 nm, indicating an increase in hardness with penetration depth. This phenomenon reminds us of previous report on nylon 6/clay nanocomposites [32], in which a gradient distribution of nanoclay induced by injection-molding was clearly evidenced by optical microscopy, XRD and thermal analysis. That is, clay concentration gradually increases from the sample surface to the inner part for the bulk specimens. This flow-induced pattern for clay distribution is usually formed and often observed during polymer melt processing. Therefore, the increase of hardness with indentation depth is probably due to a gradual increase of clay content from the surface to the center of the molded specimens.

This is even more clearly illustrated in the case of elastic modulus, which is very sensitive to the loading level of stiff inorganic clay. For modulus profiles shown in Fig. 4(B), the modulus values for all the samples steadily increase with indentation depth from 300 to 5000 nm. Besides the gradient distribution of clay nanoplatelets within the matrix mentioned and discussed above in the case of the hardness, another possible reason responsible for the increase of the hardness/modulus with the depth is probably the inhomogeneous distribution of crystallinity in the injection-molded specimens along the indentation direction. As is known, the outer part of a molded bar experiences an air-quenching process (i.e. less or no time to crystallize) upon injection molding, while the inner part undergoes a slow/long cooling process (i.e. having more time to crystallize), thus having higher degree of crystallinity than the outer portion. By DSC, the crystallinity from the surface to the core of the bulk sample for neat PA66 steadily increases from 37 to 48%. The difference in opaqueness (i.e., crystallinity) from the surface to the near surface of the injection-molded specimens can be even easily observed using naked eyes. It is well known that elastic modulus of polymers depends on the degree of crystallinity [33], consequently leading to increment of modulus with indentation depth from the surface to the near-surface of the studied samples.

Fig. 5 shows the changes of the hardness and modulus values as a function of clay concentration. The values are averaged hardness and modulus from depth between 4000 and 5000 nm. It shows a modest enhancement of hardness and stiffness with increasing clay concentration. Compared with neat PA66, the hardness increases by about 28% from 98 to 125 MPa, and the elastic modulus improves by about 18% from 2.3 to 2.7 GPa for the nanocomposite containing only 5 wt% clay. The modulus values by nanoindentation

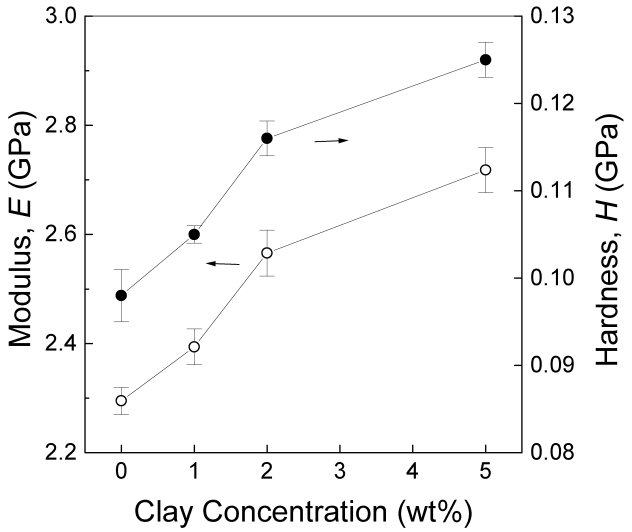

Fig. 5. Hardness and modulus of PA66 and its nanocomposites as a function of clay concentration.

are consistent or comparable with those obtained by tensile tests and DMA measurements for PA66/clay nanocomposites [26], as summarized in Table 1 for comparison. It can be seen that the modulus of neat PA66 is approximately enhanced by 20–30% with incorporation of 5 wt% clay. The origins for the discrepancy between the modulus data obtained from different methods may probably contribute to the different loading directions and the frequency used for the three measurements. For a tensile test, the loading direction is along the injection (flow) direction, in which most polymer chains are expected to align or orient in that direction. Therefore, the modulus by tensile testing normally is found to be higher than the indentation measurement where the loading direction is perpendicular to the flow direction. It is also known that for polymers, frequency used during testing will affect the viscoelastic properties of the materials. Usually, the higher frequency used, the lower modulus obtained. In DMA measurement, low frequency (e.g. 1 Hz in present study) was usually used. However, for the indentation and tensile test, the frequencies of 45 and <0.001 Hz are normally used, respectively. Thus, it is expected that the measured mechanical properties of PA66 systems have some differences from the three methods.

Table 1 also lists the moduli for the polished and unpolished samples. For the case of neat PA66, the moduli for the polished and unpolished systems are very close except that the unpolished sample has larger standard deviation. This may be due to more uncertainties, for example, higher roughness existing in the unpolished surfaces. For the case of the nanocomposites, it shows some difference between the two sets of data. The discrepancy due to the polishing effect increases with clay loading. Probably, the polishing step has removed the surface layer and exposes the inner part of the nanocomposite samples where more clay concentration and higher crystallinity make the modulus higher than the unpolished surfaces. The hardness shows similar phenomenon as observed in the case of modulus for the polished and unpolished samples.

Fig. 6 shows the plots of creep displacement versus holding time of PA66 and its nanocomposites with different clay loading. It was unexpectedly found as in Fig. 1 that, the creep amount at the maximum hold segment *increases* (i.e., decreasing the creep resistance) with increasing clay concentration. In addition, it is worth noting that the amount of creep increment from 2 to 5 wt% of clay is not that obvious. It is believed that these 'abnormal' observations are very closely related to both the morphological changes of PA66/clay nanocomposites and the enhancement effect from nanoclay, as will be discussed in detail below.

Figs. 7(A) and 6(B) show POM micrographs of neat PA66 and its nanocomposite with 1 wt% clay, respectively. Typical and well-developed spherulites with crystal size of about 50 μm are clearly observed for neat PA66, having the characteristic of a continuous sheaf-like crystalline texture aligning radically outward. Both the pronounced Maltese cross extinction patterns and the sharp boundaries of the spherulites are also seen for neat PA66. However, incorporating only 1 wt% clay into PA66 matrix greatly blurs the crystalline texture (e.g. crystal size, crystallinity) of the matrix, as observed in Fig. 7(B). And, the blurred texture even could not be defined under such a low magnification using optical microscopy. Thus, the significant change in microstructure, e.g. decreased crystal size, is most probably contributed to the decrease of creep resistance for the materials studied here.

X-ray diffraction studies further verify the above morphological observations by POM. Fig. 8 shows XRD patterns for neat PA66 and its nanocomposites as a function

Table 1
Summary of elastic modulus (E) data obtained from different measurements

Clay Content (wt%)	E (from DMA) (GPa)	E (from nanoindentation) (GPa)[a]	E (from nanoindentation) (GPa)[b]	E (from tensile tests) (GPa)
0	1.89	2.30 ± 0.02	2.27 ± 0.21	3.04 ± 0.04
1	2.22	2.39 ± 0.03	2.34 ± 0.21	3.19 ± 0.06
2	2.24	2.57 ± 0.04	2.42 ± 0.07	3.41 ± 0.06
5	2.36	2.72 ± 0.04	2.44 ± 0.32	3.91 ± 0.10

[a] Indentation modulus for the polished samples;
[b] Indentation modulus for the unpolished samples.

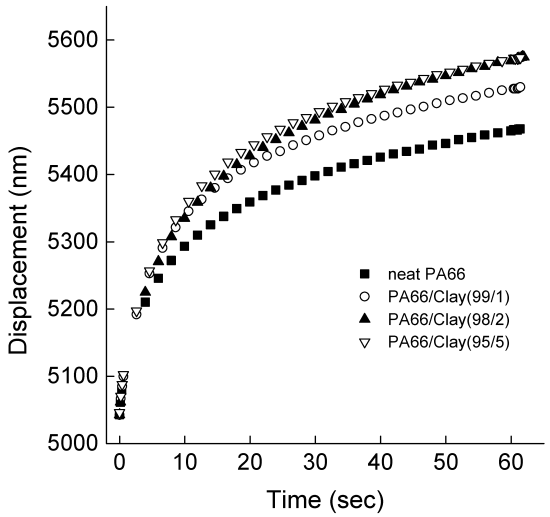

Fig. 6. Creep behavior of PA66 and its nanocomposites as a function of clay concentration.

of clay concentration. The degree of crystallinity is calculated by deconvolution of the XRD patterns, as shown in the insert of Fig. 8. Clearly, a monotonous decrease of crystallinity is seen with increasing the clay content. It should be noted that addition of only 1 wt% clay considerably decreases the crystallinity of the matrix (by about 10%), and further increasing clay concentration only has less effect (by about 5%) on the decrease of crystallinity. This is probably related to the corresponding gaps between the different plots (with different clay loading) shown in Fig. 6, thus reflecting the effect of crystallinity on the creep behavior for the studied systems. Additionally, for all the samples two strong reflection peaks, (100) and (010,110) of α-phase crystals of PA66 [34], are observed from the XRD patterns at $2\theta = 20.5°$ and 23.8°, respectively. With increasing clay content, the positions of the reflection peaks remain almost unchanged while the relative intensity of (010,110)/(100) gradually increases. This probably indicates a preferential packing of the crystals along (010,110) plane, which may be induced by incorporation of nanoclay platelets into PA66 matrix (since all the samples have the same thermal history here).

Generally, addition of clay into the polymer matrix may result in two main 'competing' or combined effects: (i) significant enhancement effect from the well-dispersed, stiff, high aspect ratio nanoclay platelets, usually and particularly having remarkable influence on hardness and modulus of the material, as observed here; (ii) substantial changes of micro- and/or nano-structures of the matrix due to confinement or other effects, for instance, the changes of crystalline morphology for semicrystalline thermoplastics owing to heterogeneous nucleation of clay particles, which usually lower or destroy the crystal perfection or crystallinity of the matrix. Probably, these two adverse effects are functioning simultaneously on the studied nanocomposite systems.

Specific to the creep behavior of PA66/clay nanocomposites studied here, it seems that at low clay loading levels

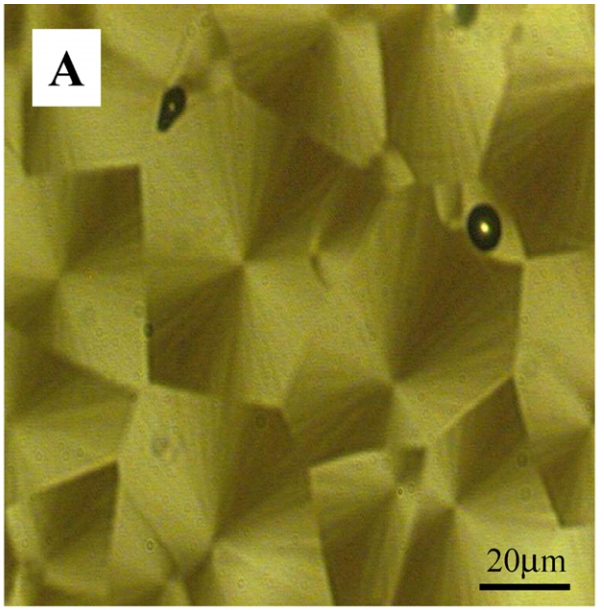

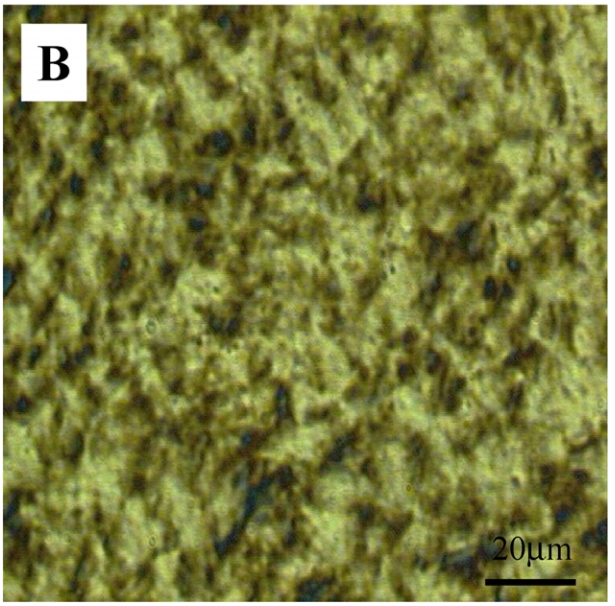

Fig. 7. Crystalline morphologies by polarized optical microscopy: (A) neat PA66; (B) PA66 nanocomposite containing 1 wt% clay.

(e.g. ≤5 wt%) the second effect plays a dominant role, that is, the increase of amorphous fraction due to clay addition leads to poor creep resistance. It is expected that with steadily increasing clay content, the (first) enhancing effect from stiff nanoclay will gradually play a dominant role in the creep behavior. And the consequence of such two competing effects may result in a critical value of clay concentration, here, 5 wt% as obtained from Fig. 6, where the plot of displacement versus hold time for the case of 5 wt% clay almost falls onto the one of 2 wt%. And most recently, Beake et al. studied the nanoindentation behavior of poly(ethylene oxide)/clay nanocomposites [16], and also

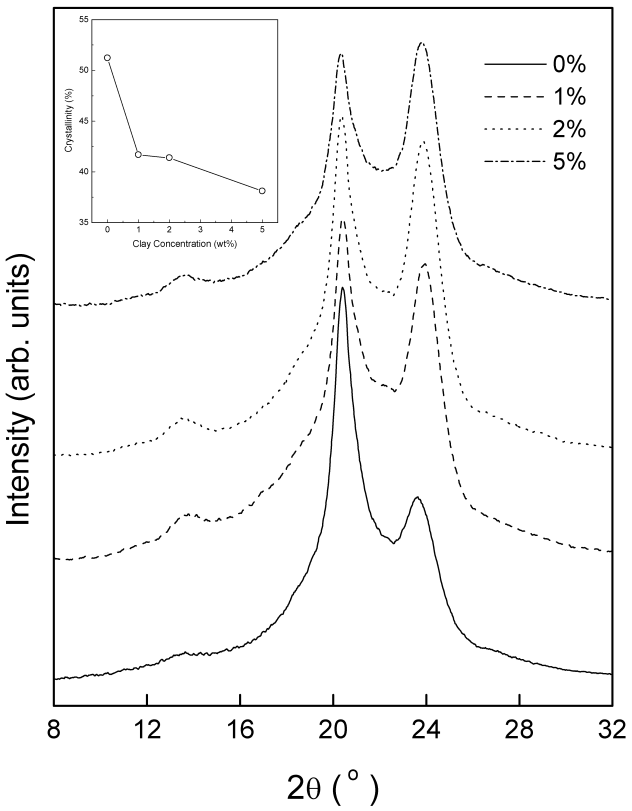

Fig. 8. XRD patterns of PA66 and its clay nanocomposites. Insert is variation of degree of crystallinity obtained by XRD as a function of clay loading.

found that the addition of small amount of clay had an adverse effect on the creep behavior of the nanocomposites, with a critical clay concentration of 5 wt% too, as observed here in PA66/clay systems. However, in their report no efforts were attempted to correlate the changes of morphology or microstructure due to clay addition with the observed creep behavior for PEO nanocomposites.

At last but not the least, it should be pointed out that another reason responsible for less creep above the critical clay concentration is probably due to the change of clay morphology. It is well documented that with increasing clay loading the intercalated population gradually dominates over the exfoliated one, as observed in many polymer/clay nanocomposites, such as in nylon 11/clay nanosystems [35]. In the intercalated cases, more polymer chains are constrained within the interlayer galleries of clay (i.e., nanoscale confinement effect), thus making the polymer chains much more difficult to move, i.e. less creep susceptibility. This speculation needs to be further verified.

4. Conclusions

In this study, the mechanical properties of nylon 66/organoclay nanocomposites have been evaluated by nanoindentation technique. The effect of clay addition on the hardness, elastic modulus and creep behavior of PA66 and its nanocomposites has been investigated as a function of clay loading. It shows that the hardness and the elastic modulus gradually enhanced with increasing clay concentration. The elastic moduli obtained by nanoindentation are comparable with those obtained from DMA measurements and the tensile tests. The effect of clay concentration on the creep behavior is significant and complex. The creep behavior of the nanocomposites is considerably increased with increasing clay content (for the cases of clay loading less than 5 wt% studied here). The creep behavior unexpectedly observed is closely related to the morphological changes occurring upon incorporating nanoclay into the matrix. The decreased crystal size and crystallinity due to the presence of clay are probably the main reasons for the increment of creep amount, which plays a dominant role on creep behavior of PA66/clay nanocomposites at lower clay loading (e.g. ≤ 5 wt% in the studied systems). The studies of the effects from other experimental parameters (for instance, strain rate, indenter geometry) on the mechanical properties of PA66/clay nanocomposites are still in progress.

References

[1] Okada A, Kawasumi M, Usuki A, Kojima Y, Kurauchi T, Kamigaito O. Mater Res Soc Proc 1990;171:45–50.
[2] Kojima Y, Usuki A, Kawasumi M, Okada A, Fukushima Y, Kurauchi T, Kamigaito O. J Mater Res 1993;8:1185–9.
[3] Lan T, Pinnavaia TJ. Chem Mater 1994;6:2216–9.
[4] Zilg C, Muelhaupt R, Finter J. Macromol Chem Phys 1999;200:661–70.
[5] Ray SS, Okamoto M. Prog Polym Sci 2003;28:1539–641.
[6] Zanetti M, Lomakin S, Camino G. Macromol Mater Engng 2000;279:1–9.
[7] Oliver WC, Pharr GM. J Mater Res 1992;7:1564.
[8] Flores A, Balta Calleja FJ. Philos Mag A 1998;78:1283–97.
[9] Briscoe BJ, Fiori L, Pelillo E. J Phys D: Appl Phys 1998;31:2395–405.
[10] VanLandingham MR, Villarrubia JS, Guthrie WF, Meyers GF. Macromol Symp 2001;167:15–43.
[11] Nowicki M, Richter A, Wolf B, Kaczmarek H. Polymer 2003;44:6599–606.
[12] Beake BD, Leggett GJ. Polymer 2002;43:319–27.
[13] Flores A, Balta Calleja FJ, Asano T. J Appl Phys 2001;90:6006–10.
[14] Krumova M, Flores A, Balta Calleja FJ, Fakirov S. Colloid Polym Sci 2002;280:591–8.
[15] Penumadu D, Dutta A, Pharr GM, Files B. J Mater Res 2003;18:1849–53.
[16] Beake BD, Chen S, Hull JB, Gao F. J Nanosci Nanotech 2002;2:73–9.
[17] Wu TM, Wu JY. J Macromol Sci Phys 2002;B41:17–31.
[18] Zhu CS, Kang X, He SQ, Wang LY, Lu LY. Chin J Polym Sci 2002;20:551–7.
[19] Liu XH, Wu QJ. Macromol Mater Engng 2002;287:180–6.
[20] Liu XH, Wu QJ, Berglund LA. Polymer 2002;43:4967–72.
[21] Yu ZZ, Yang MS, Zhang QX, Zhao CG, Mai YW. J Polym Sci, Polym Phys 2003;41:1234–43.
[22] Liu XH, Wu QJ, Zhang QX, Mo ZS. J Polym Sci, Polym Phys 2003;41:63–7.

[23] Lu YL, Zhang GB, Feng M, Zhang Y, Yang MS, Shen DY. J Polym Sci, Polym Phys 2003;41:2313–21.
[24] Han B, Ji GD, Wu SS, Shen J. Eur Polym J 2003;39:1641–6.
[25] Technical data from the website (http://www.nanocor.com) of Nanocor Inc.
[26] Phang IY, Chen L, Tjiu WC, Pisharath S, Liu TX. Mater Res Innov 2004;8(4).
[27] Sperling LH. Introduction to polymer science. New York: Wiley-Interscience; 2001.
[28] Lucas BN, Oliver WC, Swindeman JE. Mater Res Soc Symp Proc 1998;522:3–14.
[29] Ion RH, Pollock HM, Roques-Carmes C. J Mater Sci 1990;25: 1444–54.
[30] Chen L, Wong SC, Pisharath S. J Appl Polym Sci 2003;88:3298–305.
[31] Nix WD, Gao H. J Mech Phys Solids 1998;46:411–25.
[32] Liu TX, Tjiu WC, He CB, Na SS, Chung TS. Polym Int 2004;53: 392–9.
[33] Peterlin A. Colloid Polym Sci 1987;265:357.
[34] Sasgupta S, Hammond WB, Goddard WA. J Am Chem Soc 1996;118: 12291.
[35] Liu TX, Lim KP, Tjiu WC, Pramoda KP, Chen ZK. Polymer 2003;44: 3529–35.